Simultaneous control of natural and extra degrees of freedom by isometric force and electromyographic activity in the muscle-to-force null space

Sergio Gurgone[1], Daniele Borzelli[2,3], Paolo De Pasquale[2,3], Denise Jennifer Berger[3,4], Tommaso Lisini Baldi[5], Nicole D'Aurizio[5], Domenico Prattichizzo[5,6], Andrea d'Avella[2,3]

[1]Department of Matemathical and Computer Sciences, Physical Sciences and Earth Sciences, University of Messina, Messina (ME), Italy
[2]Department of Biomedical, Dental, Morphological and Functional Imaging Sciences, University of Messina, Messina (ME), Italy
[3]Laboratory of Neuromotor Physiology, IRCCS Fondazione Santa Lucia, Rome, Italy
[4]Department of Systems Medicine and Centre of Space Bio-medicine, University of Rome Tor Vergata, Rome, Italy
[5]Department of Information Engineering and Mathematics, University of Siena, Siena, Italy
[6]Humanoids and Human Centered Mechatronics, Istituto Italiano di Tecnologia, Genoa, Italy

E-mail: adavella@unime.it

Received xxxxxx
Accepted for publication xxxxxx
Published xxxxxx

Abstract

Objective. Muscle activation patterns in the muscle-to-force null space, i.e., patterns that do not generate task-relevant forces, may provide an opportunity for motor augmentation by allowing to control additional end-effectors simultaneously to natural limbs. Here we tested the feasibility of muscular null space control for augmentation by assessing simultaneous control of natural and extra degrees of freedom. *Approach.* We instructed eight participants to control translation and rotation of a virtual 3D end-effector by simultaneous generation of isometric force at the hand and null space activity extracted in real-time from the electromyographic signals recorded from 15 shoulder and arm muscles. First, we identified the null space components that each participant could control more naturally by voluntary co-contraction. Then, participants performed several blocks of a reaching and holding task. They displaced an ellipsoidal cursor to reach one of nine targets by generating force, and simultaneously rotated the cursor to match the target orientation by activating null space components. We developed an information-theoretic metric, an index of difficulty defined as the sum of a spatial and a temporal term, to assess individual null space control ability for both reaching and holding. *Main Results.* On average, participants could reach the targets in most trials already in the first block (72%) and they improved with practice (maximum 93%) but holding performance remained lower (maximum 43%). As there was a high inter-individual variability in performance, we performed a simulation with different spatial and temporal task conditions to estimate those for which each individual participants would have performed best. *Significance.* Muscular null space control is feasible and may be used to control additional virtual or robotics end-effectors. However, decoding of motor commands must be optimized according to individual null space control ability.

Keywords: electromyography, muscle-to-force null space, human augmentation, myoelectric control, virtual reality, reaching, Fitts' law

1. Introduction

Electromyographic (EMG) signals have been used for many years to control upper and lower limb prostheses [1–6], rehabilitation robotic devices [7–11], and virtual end-effectors [12–15]. Myoelectric control of a prosthetic limb by an amputee, as a replacement of the missing limb, can rely either on the detection of movement intention by EMG pattern recognition [16,17] or on the direct control of one or multiple degrees of freedom (DoFs) using EMG signals recorded from many different muscles [4,18,19]. EMG signals can be used for the control of robotic devices such as exoskeletons [20], enhancing existing abilities [21], substitute missing ones [22], or for rehabilitation after orthopedic or neurological injuries [23–25]. Myoelectric control is also a powerful tool to investigate basic principles of human motor control [12–14]. By using EMG signals to control a cursor in a virtual environment, it is possible to alter the mapping between motor commands and end-effector motion and to study how the central nervous system adapts to such perturbations. For example, a linear mapping of EMG signals onto isometric end-point forces applied to a simulated mass can be altered ("virtual surgery") such that new muscle synergies are required to compensate the perturbation [12]. Thus, to date, myoelectric control has been used mostly either to control an external device or to assist the movement of a natural limb.

Myoelectric control, however, could also be used to control an external device concurrently with the motion of the natural limbs, possibly augmenting human motor capabilities. At the basis of augmentation lies the concept of motor task null space. Due to the redundancy of the musculoskeletal and neural systems, i.e., the presence of a higher number of active units (muscles and neurons) than the end-effector degrees of freedom involved in a task, many combinations of joint angles, muscle patterns and neural signals do not generate task-relevant movements or forces [26]. Such combinations lie in the kinematic, muscular and neural null space respectively. A few approaches for augmentation based on these concepts have been recently investigated. Abdi and collaborators [27] developed three-handed manipulation in a virtual environment, using the motion of a foot to control the third hand in a simple task. Similarly, a third robotic thumb controlled using a toe [28] and a sixth finger controlled through kinematic null space of upper limbs [29] have been developed and tested. Salvietti and collaborators [30] also demonstrated that it is possible to control a supernumerary robotic finger using EMG signals from frontalis muscles, while Parietti and Asada [31] controlled an extra robotic leg using EMG signals from torso muscles. In most cases, however, kinematic or muscular signals used for controlling additional DoFs have been recorded from body parts not directly involved in the task performed concurrently with the DoFs of the natural limbs. In many real-life conditions, however, such body parts may be involved in the task and thus may not be available to control extra DoFs. Finally, concerning neural null space, a non-invasive brain-machine interface has been used to control a third arm for multitasking [32], but not all participants were able to achieve multitasking.

Here we propose a novel approach to motor augmentation based on the concept of task-intrinsic muscular null space. Muscular null space is the vector space of muscle activation patterns that do not generate net joint torques (e.g., the co-contraction of two antagonistic muscles, which counterbalance the effect of each other). In many real-life motor tasks, muscular null space is associated to the control of end-effector impedance, especially in presence of unstable interactions with the environment [33–35]. Thus, muscular null space has been successfully used for tele-impedance application, i.e. the control of the impedance of robotic devices through human impedance [36,37]. However, muscular null space can also be used to control extra DoFs. Borzelli and collaborators have demonstrated that muscular null space can be controlled voluntarily to modulate the stiffness of a virtual end-effector during the generation of multidirectional isometric forces [38]. Takagi and collaborators [39] have shown that it is possible to regulate co-contraction of two antagonist muscles to control the vertical position of a 2D cursor while simulaneously controlling the horizontal position with reciprocal activation. Bräcklein and collaborators [40] have successfully proved that beta band activity in the neural drive to a muscle, which does not directly affect the force generated by that muscle, can be modulated to control a cursor in a 2D environment. However, no study to date has used null space signals extracted from many muscles to directly control extra DoFs while simultaneously performing a task in 3D environment involving multiple DoFs controlled by the same muscles (i.e., using the "task-intrinsic null space), thus augmenting human motor abilities. This approach differs both from the use of task-extrinsic null space, i.e., from body part not directly involved in the task, and from tele-impedance control.

In this study, we aimed at testing the feasibility of task-intrinsic muscular null space control for motor augmentation by assessing the performance of participants in the simultaneous control of natural and extra DoFs. Moreover, we aimed at assessing whether and how fast null space control ability improves with practice. We designed an experimental protocol in which participants had to displace a cursor in a 3D virtual environment to reach 8 targets by generating isometric force and simultaneously to control an extra DoF, i.e., the rotation around one axis of the cursor, which had an ellipsoidal shape, through null space activation in arm and/or shoulder muscles. Participants were also instructed to hold the cursor at the target for a given time interval. Thus, our protocol required the simultaneous control of natural and extra DoFs to perform both a spatial and a temporal task.

To quantify participants' performances and to understand how the task could be optimized to match individual control ability, we used a novel index of difficulty (ID), an information-theoretic metric inspired by Fitts' law. Although Fitts' law general validity has been frequently questioned in the past, Gori and collaborators [41] have proposed an information-theoretic model of the human motor system for pointing tasks, where the ID is the information about the selection of a target transmitted through a noisy channel. To date, many researches in human motor control used measures derived from the Fitts' law to evaluate performance in different tasks [42–44]. However, the possibility of considering the time as a "target" itself, i.e., the application of the Fitts' law to temporal control, has been rarely studied [45]. To address this issue, we introduced an ID defined as the sum of a spatial term, related to difficulty in selecting a target by reaching it (i.e., quantifying spatial control ability), and a temporal term, related to the difficulty in holding the target for a given time interval (i.e., quantifying temporal control ability).

2. Materials and Methods

2.1 Participants

Eight naïve right-handed participants (mean ± SD age: 27.4 ± 7.8 years, age range: 20–45, 2 females) participated in the experiments after giving written informed consent. All procedures have been conducted in accordance with the principles embodied in the Declaration of Helsinki, comply with national regulations, and have been approved by the ethics committee IRCCS Sicilia - Sezione Neurolesi "Bonino-Pulejo" (Prot. n. 02/18). All participants had normal or corrected to normal vision and did not report any known neurological disorder or upper right limb injury.

2.2 Setup

The setup used for this work is similar to that used in previous studies [12,38,46]. Participants sat on a gaming chair in front of a desktop (Fig. 1A), with the right hand inserted in an orthosis rigidly connected to a 6-axis force transducer (Delta F/T Sensor, ATI Industrial Automation, Apex, NC, USA). Arm and forearm formed a 90° angle, and the chair was positioned so that the hand was at level of the solar plexus. Car belts immobilized the participant's torso and shoulders. Shutter glasses (GeForce 3D Vision 2, NVIDIA Corporation, Santa Clara, CA, USA), allowed to view stereoscopically a three-dimensional scene displayed on a horizontal mirror, placed over the participant's hand, reflecting the image visualized at 120 Hz (60 Hz for each eye) on a monitor. The scene included a virtual desktop and a cursor (spherical or ellipsoidal) whose position matched the position of the center of the palm when no force was exerted. Real-time feedback of the exerted force was provided as the displacement of the cursor. Cursor motion in three-dimensional space was simulated as an adaptive mass-spring-damper system, subject to the force applied by the participant on the orthosis. The spring constant was set such that the force applied to maintain the cursor stationary at the target was equal to a specific fraction of the magnitude of the participant's maximum voluntary force (MVF, see below). The mass was adjusted adaptively in the range 15–140 g as a sigmoidal function of the rate of change in the magnitude of the recorded force, to maintain fast responses to changes in force while reducing the effect of noise with stationary force [12].

Surface EMG activity was recorded from fifteen muscles acting on the shoulder and elbow: brachioradialis, biceps brachii long head and short head, pectoralis major, anterior deltoid, middle deltoid, posterior deltoid, triceps brachii lateral head and long head, infraspinatus, teres major, latissimus dorsi, lower trapezius, middle trapezius, and upper trapezius. The signal was acquired at 1000 Hz with active wireless bipolar surface electrodes (Trigno System, Delsys Inc., Natick, MA, USA), bandpass filtered (20 – 450 Hz), and amplified with a gain of 1000. Participants' skin, in correspondence to the target muscles, was cleansed with alcohol and electrodes were placed based on recommendations from SENIAM [47] and by palpating muscles to locate the muscle belly and orienting the electrodes along the main direction of the muscle fibers.

Experiment control, data acquisition, and data analysis were performed with custom-written software in MATLAB® (MathWorks Inc., Natick, MA) and Java®.

2.3 Experimental protocol

After an initial familiarization with the experimental setup, participants performed 18 blocks with different task conditions. In the first block (MVF estimation), they were instructed to exert their MVF directed towards their chest on the horizontal plane (-*y*, with *y* away from the chest along the anteroposterior axis). The maximum of the force recorded in this block was used to normalize target distance in the following blocks. Using data previously collected with a similar protocol [48], we verified that such estimation of MVF was highly correlated to the average maximum force across multiple horizontal directions.

In the second block (force control, FC), participants were instructed to move, both accurately and quickly, a spherical cursor from the rest position to a target (Fig. 1B), located in one of twenty spatial positions around the rest position, by applying isometric forces on the orthosis. At the beginning of each trial (*rest phase*) participants were asked to relax their right arm muscles to maintain the cursor inside a transparent sphere at the centre of the scene, i.e., the rest position, for 1 s. Then, a transparent sphere appeared in one of the twenty target positions (*target go event*), placed on the vertices of a dodecahedron inscribed into a sphere, centred in the rest position, and whose radius was either 15% or 25% the MVF. Participants were asked to reach the target and remain within the target sphere (see Fig. 1B), whose radius exceeded that of the cursor by 2% the MVF, for 0.5 s (*holding phase*). When the cursor was within the target tolerance, the target changed color (from gray to yellow). Each target was presented three times, such that each participant performed a total of 120 trials (20 targets × 2 radii × 3 repetitions, presented in random order). The time limit for trial completion was 4 s. EMG and force data collected from the target go event until the first time the cursor entered the target (*dynamic phase*) were used to estimate a subject-specific matrix that approximates the mapping of EMG activations onto isometric force (see below *EMG-to-force matrix*) and its null space. The maximum amplitude of each EMG signal (low-pass filtered with second-order Butterworth after rectification; 1 Hz cutoff) collected during the same phase, first computed for each trial, was averaged for each target and then the maximum across all the target directions was used to normalize EMGs during the rest of the experiment. After this block, there was a 5 min pause to process the data.

In the third block (null space modulation, NSM), participants performed a cursor stabilization task that required voluntarily modulation of muscular co-contraction. The EMG data collected in this condition were used to estimate the null space patterns that each participant generated more naturally. Participants had to maintain, using muscular null space activations, the cursor inside a target placed at the rest position, whose radius exceeded that of the cursor by 6% of the MVF, for 1 s while a simulated force perturbed its motion. The perturbing force was the sum of three sinusoidal forces acting along the three dimensions and with frequencies (38 Hz for the *x* component, 30 Hz for the *y* component, and 46 Hz for the *z* component) too high to be tracked by voluntary modulation of force production. The motion of the cursor was simulated in real-time as a mass-spring-damper system with a stiffness related to the amount of co-contration (see "Cursor control during the NSM block" section below; further details can be found in [38]). To reduce this oscillation, participants were instructed to co-contract their right arm and/or shoulder muscles, as they prefer and feel more natural, without any other constraint except the generation of zero force. The time limit for trial completion was 15 s, with 5 s of pause between trials. As for the FC block, visual feedback of the cursor being within target tolerance was provided by changing the color of the target. EMG data collected during the holding phase were used to calculate the null space directions to be used for the control the extra degree of freedom (see "Selection of null space control variables" Appendix in Supplementary Material).

In the fourth block (isometric reaching with ellipsoidal force control, EFC), participants performed an isometric reaching task with ellipsoidal, rather than spherical as in the FC block, cursor and targets. There were eight targets (3 repetitions), each placed on the *x*-*y* plane at 20% of MVF from the origin, with a tolerance of 2% of MVF, and equally distributed with a 45° angular distance one from the other (0° = +*x* direction, with *x* mediolateral axis pointing to the right; in the analysis, target 1 has been considered the one with *x* = +20% of MVF and *y* = 0, with the others following in counter-clockwise rotation). This block provided a baseline reference for the following 12 blocks.

In blocks 5th to 16th (null space control, NSC), participants were instructed to both translate and rotate the ellipsoidal cursor (around the intermediate axis of the ellipsoid which was rotated such that it was parallel to the longitudinal axis of the forearm) to match the position and orientation of the target (Fig. 1C). Translation was achieved by exerting force and rotation by generating muscle patterns with a component aligned to specific null space directions, identified using the data collected in the NSM block (see "Selection of null space control variables" Appendix in Supplementary Material). Each block was composed of three repetition of trials with nine targets (Fig. 1D) in different *x*-*y* positions – the same eight as in the EFC block plus one in the rest position – and with the same orientation corresponding to a 60° rotation of the ellipsoidal cursor from the rest orientation and a tolerance of 7.2° (4% of 180°). The target orientation could be achieved with a null space activation norm of 20% of the maximum norm recorded during NSM block ("maximum voluntary co-contraction", MVCC). The translation tolerance was also 4% of MVF. Participants were instructed to hold the cursor at the target for 1 s. In this case, the target changed color only when the cursor was within spatial and angular tolerances simultaneously. The nine targets were presented in a random sequence (cycle). The time limit for trial completion was of 4 s. At the end of each cycle, the score for that cycle was visualized.

The 17th block was a null space control block without visual feedback (hidden NSC), and was meant to assess the level of retention of null space control without visual feedback.

Finally, the 18th block was an additional EFC block. A schematic of the experimental protocol is presented in Fig. 1E.

2.3.1 EMG-to-force mapping

In isometric conditions, i.e., when muscles generate force without reducing or increasing their length, as in our experimental protocol, and when the force exerted is submaximal, the relationship between muscle activation and force exterted at the hand can be approximated by a linear mapping:

$$\boldsymbol{f} = \boldsymbol{H}\boldsymbol{m},$$

where $\boldsymbol{f}$ is the tridimensional force vector, $\boldsymbol{m}$ is the 15-dimensional muscle activation vector, and $\boldsymbol{H}$ is the EMG-to-force matrix that maps muscles activations onto force. The matrix $\boldsymbol{H}$ was estimated using multiple linear regressions of each force component, low-pass filtered (second-order Butterworth; 1 Hz cutoff), with EMG signals recorded during the dynamic phase of the first force control block, low-pass filtered (as the force, but after rectification) and normalized to the maximum EMG activity recorded during the force control block targets at 25% of the MVF distance. We verified that the $\boldsymbol{H}$ matrix estimated using holding phase data was similar to the one extracted using dynamic phase. In fact, the angle between the force vectors of the dynamic phase $\boldsymbol{H}$ matrix and the holding phase $\boldsymbol{H}$ matrix for the same muscle was 23° ± 34°

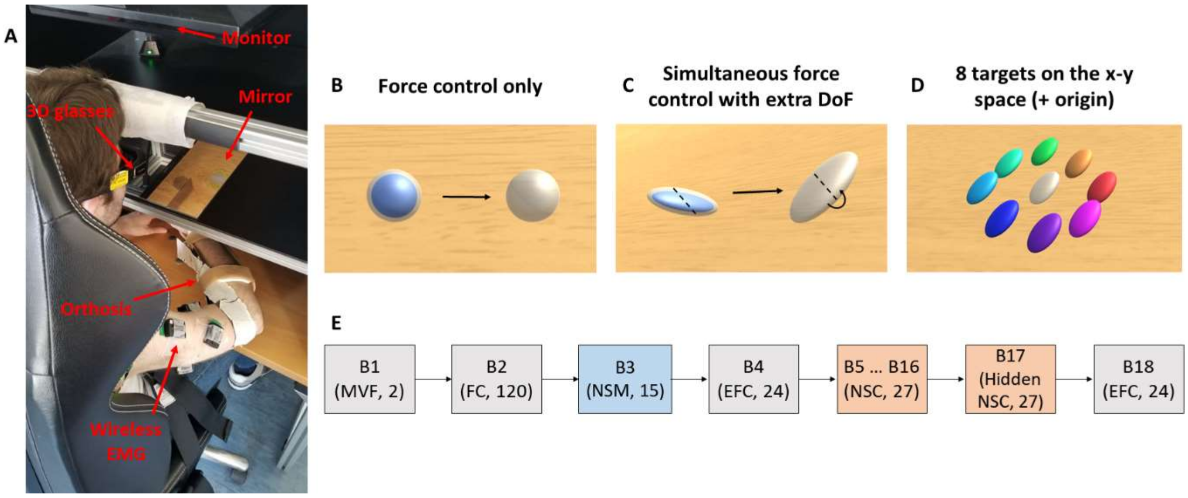

Figure 1. Experimental setup and protocol. (A) Experimental setup: a 3D virtual scene is projected stereoscopically on a horizontal mirror occuding the participant's hand, which is attached through an orthosis at a force transducer (below the desktop, not visible); wireless sensors are used to collect EMG activity from shoulder and arm muscles. (B) Illustration of the task during force control blocks (the blue cursor moves in the direction of the arrow). (C) Illustration of the task during null space control blocks (the dashed lines represent the rotation axis). (D) Target arrangement. (E) Experimental protocol schematic (MVF = maximum voluntary force, FC = force control, NSM = null space modulation, EFC = ellipsoidal force control, NSC = null space control; the number after the block abbreviation is the number of trials).

(median value ± interquartile range across muscles and participants).

The matrix $\boldsymbol{H}$ was also used to compute the null space matrix $\boldsymbol{N}$, i.e., a matrix whose columns constitute an orthonormal basis for the subspace of EMG activation vectors $\boldsymbol{m}_0$ that are mapped by the $\boldsymbol{H}$ matrix onto the null force vector:

$$0 = \boldsymbol{H}\boldsymbol{m}_0.$$

2.3.2 Cursor control during the NSM block

In the NSM block, the perturbation was generated as a sinusoidal force (with different frequencies along different axes) acting on a mass attached to a position (controlled by force) through a spring with an elastic constant that was adjusted in real time according to the norm of the null space activation vector through a logistic function [38]:

$$k(\boldsymbol{n}) = \frac{k_{max}}{e^{-r_k(\|\boldsymbol{n}\|-\|\boldsymbol{n}_0\|)}+1},$$

where $\|\boldsymbol{n}\|$ is the norm of the null space activation vector, $k_{max} = 9500\ N/m^2$ is the spring constant, r_k is a variation rate parameter, and $\|\boldsymbol{n}_0\|$ is the value of the null space norm such that $k(\boldsymbol{n}_0) = \frac{k_{max}}{2}$. The value of $\|\boldsymbol{n}_0\|$ was set equal to 2.5 times the minimum norm ($\|\boldsymbol{n}_{min}\|$) of the mean null space activation during the holding phases of FC block, while r_k was calculated using the formula:

$$r_k = -\log\left(\frac{k_{max}/y_0 - 1}{x_0 - 1}\right),$$

where $(x_0, y_0) = (\|\boldsymbol{n}_{min}\|, 500\ N/m^2)$. These parameters limited the cursor oscillation when participants had their muscles relaxed, but assured an adequate reduction of the oscillations when participants were actively co-contracting. Therefore, these parameters were chosen to ensure that the level of co-contraction observed in each participant was effective in modulating the stiffness of the virtual end-effector.

2.3.3 Control of the extra degree of freedom by null space variable

To characterize the subject-specific directions in the EMG null space to be used for the control of the extra DoF, each participant performed a NSM block. This procedure allowed to identify the directions that each participant could control more naturally and the dimensionality of this subspace. We then selected the directions in the null space with the largest amplitude modulation of null space activation during the NSM block and used the projection of the instantaneous muscle activity vector onto those directions as the signal to control the extra DoF (mean value of components ± SD among participants: 2.1 ± 0.8, range 1-3).

The mapping of null space activation into a control variable was selected in a preliminary study (see "Selection of null space control variables" Appendix in Supplementary Material). We used data collected during simultaneous force production and null space modulation in a different study [38] to compare three different methods. We selected as control variable (f_{DoF}) the norm of the projection of the null space activation vector $\boldsymbol{n}$ onto the first nc principal components that explain 80% of variance of NSM block data after subtraction of the mean vector of null space activation in baseline FC block $\bar{\boldsymbol{n}}_{bl}$, taken as a reference of residual, involuntary null space activation:

$$f_{DoF} = \|\boldsymbol{V}_{cc}(:,nc)^T[\boldsymbol{n} - \bar{\boldsymbol{n}}_{bl}]\|;$$

where $\boldsymbol{V}_{cc}(:,nc)^T$ represents the transpose of the first nc columns of the matrix of the principal components of the null space activation vectors collected in the NSM block.

We then mapped the null space control variable onto the extra DoF according to a logistic function, similar to the one used in the NSM block, because it is positive defined, and participants could then reach the rest position simply by relaxing their muscles. Moreover, it has a smooth and continuous derivative, so that there is no need for thresholding, as it would have been necessary for example with a linear function.

Therefore, the control law that mapped the null space control variable onto cursor rotation angle was defined as:

$$\theta(f_{DOF}) = \frac{\theta_{max}}{e^{-r_\theta(f_{DoF}-f_{DoF,0})}+1}, \quad (3)$$

where θ is the angle of rotation, θ_{max} is the maximum angle of rotation, set to 145°, r is the variation rate, f_{DoF} is the control variable and $f_{DoF,0}$ is the value of the control value for which $\theta(f_{DoF}) = \frac{\theta_{max}}{2}$.

The value of $f_{DOF,0}$ was computed using n equal to 25% of the MVCC. The r_θ value was calculated using the formula:

$$r_\theta = -\log\left(\frac{\theta_{max}/y_0 - 1}{x_0 - 1}\right),$$

where $(x_0, y_0) = (f_{DoF}(\boldsymbol{n}_{min}), 0.1^\circ)$.

2.4 Data Analysis

All collected data were visually inspected and trials in which EMG artefacts were detected were discarded. The discarded trials were 13.1 ± 7.6 (mean ± SD over participants) over a total of 536 trials performed by each participant. Trials in the NSC blocks with the target in the central position (i.e., requiring only cursor rotation) were not included in the analysis.

2.4.1 Task performance

Task performance was evaluated both as the fraction of trials per block in which participants reached the target (*reaching success rate*), and as the fraction of trials per block in which participants held the cursor in the target for the required time (*holding success rate*).

Mean holding time and mean angular error per block were also calculated. In each trial, *holding time* was defined as the longest time interval in which the cursor remained inside the target (maximum value 1 s, the required holding time). The *angular error* was defined as the mean of the absolute value of the difference of the cursor rotation angle and the target rotation angle over the interval in which the cursor position error in space was under the threshold of 6% of MVF. It was calculated for both NSC blocks and the hidden NSC blocks, however, due to the low performance in reaching (mean ± SD over participants: 4 ± 8 %), we decided to not perform any analysis on this block due to low availability of trials.

To address the issue of muscular fatigue, we calculated the Welch's power spectral density of the raw EMG data for each participant, cycle and muscle (using MATLAB function *pwelch*). For each muscle, we considered only the target with the highest average activation across blocks. We then calculated the median frequency, i.e., the frequency that separates the power spectrum into two parts of equal energy. It is known from literature that an increase in the median frequency indicates the occurrence of fatigue [49,50]. We performed a linear regression of the median frequency for each muscle and participant as a function of cycle, and we found that an average of 3.5 ± 2.7 muscles (mean ± SD among participants) presented a significant fit with positive slope. This indicates that fatigue could have affected individuals performance and learning.

2.4.2 Velocity peaks and movement strategies

Two different velocities of the cursor were calculated: the tangential velocity of the cursor spatial position (therefore related to the force), and the angular velocity of the cursor (therefore related to the muscle null space activation).

The two velocities were computed numerically for each trial, after applying a 2nd order Butterworth filter (3 Hz low-pass cutoff frequency) to the cursor position (measured as fraction of MVF) and to the cursor rotation angle. The *movement onset* was defined as the first sample after the end of the rest phase (i.e., when the target appeared on the screen) at which the cursor velocity was higher than a threshold equal to three times the mean velocity recorded in the 0.5 s before the 'target go' event, which is generally equal to zero due to the participant being at rest, but could be greater than zero due to oscillations or noise. The *peak velocity* was defined as the first maximum after the movement onset.

Movement onset and velocity peaks were analyzed to assess if different participants used different movement strategies. For example, if a participant displaced the cursor first and then rotated it (using muscular null space activation), or vice versa, or if they moved and rotated the cursor simultaneously, or if there was no specific relation between the two movement components.

2.4.3 Performance analysis

In addition to success rates, we used information theory to assess individual control ability. We considered the information about the instructed target and time interval that is transmitted by each participant when performing a reaching and holding movement. To generalize the assessment of individual ability beyond the performance achieved by each participant with the specific parameters of the experimental protocol (e.g., the target size or the required holding time) we estimated, through a simulation, the information that would have been transmitted with different target sizes and holding times.

The information transmitted accomplishing a reaching task may be quantified by an *index of difficulty*, as introduced by Fitts [51]. The Fitts' law states that movement time MT in a reaching task is linearly related to an index of difficulty ID:

$$MT = a \cdot ID + b.$$

The Fitts' ID, for a target of width W and distance D from the origin, in the Shannon-MacKenzie formulation [52], is equal to:

$$ID = log_2\left(\frac{D}{W} + 1\right).$$

While Fitts' law validity has been questioned because of its unclear theoretical foundations [53,54], Gori and collaborators [41] derived this law with a simple model of the human performance of an aiming task as a communication process. In this model, the source of the message is the target the individual intends to reach ("aiming is choosing"). In the original formulation of Fitts, aiming at a target of width W at distance D is equivalent to selecting one of n linearly arranged targets of width W such that $D = nW$ (Fig. 2A). If the targets can be selected with the same probability, the entropy of the target distribution, i.e., the entropy of the source, is equal to the ID. The message is then sent through a noisy channel, representing the execution of the reaching movement with physiological noise in the neural and the musculoskeletal systems. If the noise results in a distribution of the arrival position with an amplitude less than $W/2$, aiming at the center of the target allows to always hit the selected target and thus transmitting the message without error. Then, the ID quantifies the information that can be transmitted in an aiming task with negligible error rate, equal to the source entropy for errorless transmission. Apart from its theoretical framework, Fitts' law has been shown to be a robust empirical relation between movement time and the spatial parameters of a task as long as no temporal constraints are set, or if these constraints are relaxed in such a way that they do not influence too much the task itself [55–57].

Since in our task subjects were required to reach the spatial location (*xyz* coordinates) of the target and to align the cursor to the target orientation, we can define two distinct indices of difficulty for each one of the two components of the reaching movements (translation and rotation). For the 3D displacement of the cursor position, considering that the tolerance is always the same for the three axis, a *displacement* ID can be defined as:

$$ID_{xyz} = log_2\left(\frac{D}{W_{xyz}} + 1\right) = log_2\left(\frac{D}{2R} + 1\right),$$

where D is the target distance in % of MVF, and R is the target radius also in % of MVF.

Recent research has shown a dependence of the movement time on the target angle for 2D and 3D tasks [58,59]. According to our data, the dependence resembles a linear combination of a sine term and a cosine term. Therefore, a better definition of the ID is:

$$ID_{xyz} = log_2\left(\frac{D}{2R} + 1\right) + c \cdot \sin(\alpha) + d \cdot \cos(\alpha),$$

where α is the direction angle of the target on the *x-y* plane. The two coefficient c and d were calculated by fitting movement times vs ID_{xyz} in the two EFC control blocks.

For the cursor rotation, a *rotation* ID can be defined as:

$$ID_{\theta} = log_2\left(\frac{D}{W_{\theta}} + 1\right) = log_2\left(\frac{\theta}{\Delta\theta} + 1\right),$$

where θ is the rotation angle and $\Delta\theta$ is the rotation angle tolerance (Fig. 2B). The total *spatial* ID can then be defined as the sum of the displacement and rotation indices:

$$ID_S = ID_{xyz} + ID_{\theta}.$$

The application of this ID formulation to our experimental protocol raises three issues. First, Fitts' law has been formulated for an aiming task in which the participant is not required to hold the end-effector at the target location for a specific time interval, but rather to simply hit the target. However, when considering the control of an end-effector with myoelectic signals, it may be necessary to provide also a temporal command in addition to a spatial one. Because myoelectric control is typically noisier than the natural limb control, it would be then useful to quantify also the target holding performance. Second, the Fitts' law does not consider the actual error rate in the reaching task, assuming that it is low enough to be neglected. This second issue has been addressed by estimating an effective target width for which the error rate is below a given small (but arbitrary) threshold [44,60,61]. However, individual ability in aiming at a target can be rigorously quantified using a communication model with transmission errors [41]. Third, to properly assess the individual ability to control the position and orientation of the cursor, we should have used targets of different size and different holding time requirements. Indeed, speed-accuracy trade-off functions derived by systematically varying the required accuracy have been used to assess individual skill in manual tasks [62,63]. However, an additional factor in our experimental design would have required a large number of trials making the assessment too long and fatiguing. We therefore opted for an approximate but faster assessment of the dependence of the individual cursor control ability on the specific task parameters by simulating off-line the performance that would have been achieved with different parameters.

Concerning the first issue, we followed the model of a communication system to derive also a *temporal* ID. Making a parallel with the spatial case, in which we have *n* targets of width W in a length D, we can consider a time interval of duration T, which can be divided in n consecutive temporal targets of duration Δt. In this way, in addition to selecting a spatial target by reaching it, it is possible to select one of the temporal targets by holding at the spatial target until the specific time is elapsed. In addition to considering that "aiming is choosing" (Fig. 2A and B) [41], which means that an individual can choose one target from a set of many by aiming at it, we consider that "waiting is choosing" (Fig. 2C), which means that an individual can choose a "temporal target" from a set of many by waiting for a given time interval before moving. Following this reasoning, an expression for a temporal index of difficulty can be derived as:

$$ID_T = log_2\left(\frac{T}{\Delta t} + 1\right),$$

where T is the duration of the considered time interval, while Δt is the duration of the time sub-intervals, defining the required temporal accuracy.

Concerning the second issue, many attempts have been done to calculate the effective size of the target that would satisfy the assumption of negligible error rate, such as the one from Welford [60], which however has been criticized because it is based on questionable assumptions [41]. Therefore, Gori and collaborators have proposed a new corrected index of difficulty that takes into account the error rate. It can be derived using a compound channel with two states (a good state and a bad state), as the Shannon-MacKenzie ID multiplied by the success rate $(1-\varepsilon)$:

$$ID(\varepsilon) = (1-\varepsilon) \cdot log_2\left(\frac{D}{W}+1\right).$$

In our case, we considered the reaching error rate ε_r (or the success rate $(1-\varepsilon_r)$) related to the identification of the target in space, i.e., to the spatial ID, while the holding error rate ε_h (or the success rate $(1-\varepsilon_h)$) to the identification of the time interval, i.e., to the temporal ID. Therefore, the corrected ID can be defined as:

$$ID(\varepsilon_r, \varepsilon_s) = (1-\varepsilon_r) \cdot ID_S + (1-\varepsilon_h) \cdot ID_T.$$

Concerning the third issue, in our experimental protocol we used only one target size (corresponding to a cursor translation accuracy of 4% MVF), and one cursor rotation tolerance (corresponding to 4% of the MVCC). Moreover, the temporal accuracy required for the holding time (the Δt parameter) was not explicitly defined: partipants were required to keep cursor in position inside targets for a time $T = 1\ s$. However, since we wanted to assess the individual ability in displacing and orienting the cursor and in holding the target regardless of specific task parameters, we used the data collected in one condition to simulate the performance that participants would have achieved in different conditions. Thus, we computed the reaching performance with targets of different sizes (6% to 3 % of MVF and corresponding % of MVCC, with a step of 0.5%), and the performance for holding the target for the required time with differenent temporal tolerances (1 s ± 0.1 s to 1 s ± 0.9 s with a step of 0.1 s, and 1 s ± 0.999 s, this last being equivalent to just spatial reaching).

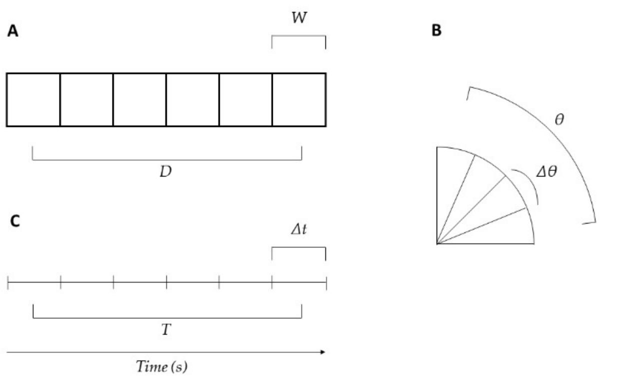

Figure 2. Spatial and temporal ID definitions. Schematic representation of target patterns, according to the Shannon-MacKenzie formulation of the ID, for the three indices: (A) displacement, (B) rotation, and (C) time.

As a first step, we estimated the mean reaching movement time MT_R (defined as the time interval between the “target go” event and the first time the cursor entered the target) and the mean execution movement time MT_E (defined as the time interval between the “target go” event and the end of the holding phase) from simulations with different target size and holding time (for MT_E only) tolerances for each participant. The simulation was performed by measuring if a target of a specific size would be hit by a participant with the real trajectories recorded during task execution, and how much time a participant kept the cursor inside the specified space region according to the real trajectories. Then, we linearly fitted reaching movement times vs reaching IDs (in the form: $MT_R = a_S \cdot ID_S + b$, where a_S and b are the fitted parameters) to verify that our data follow Fitts’ law, and execution movement times versus total IDs (in the form: $MT_E = a_{S'} \cdot ID_S + a_T \cdot ID_T + b'$, where $a_{S'}$, a_T and b' are the fitted parameters) to verify that a linear relation still holds when the temporal ID is added.

Finally, an additional measure of performance that can be obtained from the Fitts’ law is the *throughput*, defined as the ratio between the ID and the movement time. The average movement times for each block and target were taken, and the mean across targets was computed. We then estimated the throughput considering only the reaching phase, because the holding phase has a fixed information rate. Whenever a target was not reached in a block, we set the throughput for that target to zero.

2.4.4 Statistical Analysis

Statistical analysis was performed using MATLAB. Kruskal-Wallis one-way ANOVA (function *kruskalwallis*), after Anderson-Darling test (function *adtest*), was used to compare reaching and holding success rates for all targets, and the R^2 of reconstruction of the three force control blocks (one FC and two EFC blocks).

For the NSC blocks, the dependence of reaching and holding success on cycle and target was assessed by fitting a generalized linear mixed model (function *fitglme*), with the cycle (3 cycles per block) and target (8 peripheral targets) as fixed effects and participant as random effect. Similarly, the dependence of angular deviation and holding time on cycle and target was assessed by fitting a linear mixed model (function *fitlme*). Additionally, a generalized linear model function *fitglm*) and a linear model (function *fitlm*) were fitted to the response variables for each participant separately.

Pearson correlation coefficient (function *corrcoef*) between force and extra DoF peak velocity times was calculated to assess the correlation between the two velocity peak times across blocks, and Kruskal-Wallis one-way ANOVA, after Anderson-Darling test, was used to evaluate differences between the dataset distributions.

3. Results

3.1 Force control performance

We recruited eight participants to assess their ability to control simultaneously natural and extra DoFs. We first assessed baseline performance in FC. During this block, participants displaced the cursor toward the targets along approximately straight paths, reached the target successfully in 92 ± 6 % (mean ± SD across participants) of the trials, and remained in the target for the required time in 63 ± 19 % of the trials (see Table 1 for individual data). Thus, while reaching the target was easily accomplished by our participants, holding was more challenging. Moreover, holding performance varied considerably across participants, as indicated by its large standard deviation. Similar performances were observed during the initial EFC block, for which the success rates for reaching and holding were, respectively, 88 ± 25 % and 67 ± 31 %. No significant differences were found between FC and EFC blocks for both reaching and holding performance ($p = 0.24$ and 0.56 respectively, Kruskal-Wallis one-way ANOVA). Therefore, the shape (spherical or ellipsoidal) of cursor and targets did not affect force control performance.

The mean R^2 across participants of the tridimensional force reconstruction during the FC block, was 0.76 ± 0.11 (see Table 1 for individual data). During the initial EFC block, the mean horizontal (rather than tridimensional, as targets were all planar in this block) force reconstruction R^2 was 0.78 ± 0.13, and no significant differences were found with respect to the initial FC ($p = 0.46$, Kruskal-Wallis one-way ANOVA). These results support the robustness of the EMG-to-force mapping, which was used for calculating the EMG null space and therefore the variable used to control the extra DoF.

Participant	**Reaching success rate**	**Holding success rate**	**Force reconstruction R^2**
1	0.92	0.59	0.85
2	0.88	0.42	0.52
3	0.96	0.51	0.74
4	0.96	0.78	0.75
5	0.89	0.46	0.79
6	0.97	0.72	0.84
7	0.83	0.56	0.70
8	0.99	0.98	0.89

Table 1: individual performance and quality of force reconstruction by EMG-to-force linear mapping for the FC block.

3.2 Simultaneous force and null space control performance

In NSC blocks, participants performed trials with eight ellipsoidal targets, positioned at a distance and with an orientation corresponding to 20% of MVF and 20% of MVCC respectively. Additional trials with the target at the rest position and orientation corresponding to 20% of MVCC, i.e., requiring only cursor rotation, were not included in the analysis.

Differently from FC and EFC blocks, especially in the initial NSC blocks, cursor trajectories were highly variable over repetitions because of the interference between the natural and extra DoFs and the lack of coordination among them. Although participants directed the cursor quite accurately toward the targets, they were less accurate with the cursor rotation (i.e., the extra DoF), which was controlled by null space activation, and the rotation angle often overshoot the target angle and oscillated around it. This is clearly visible in both panels of Fig. 3, where in the first blocks the extra DoF often exceed the upper target threshold (*dashed horizontal line*). Interference between force and null-space control sometimes also led to an oscillation in the spatial position of the cursor, highlighting the difficulty in simultaneous control of the different DoFs, as it is visible in panel A of Fig. 3. With practice, however, all participants improved in their control of the extra DoF. For example, for all three participants illustrated in Fig. 3 initially (Block 5, *blue lines*) the first peak velocity of cursor rotation (*vertical lines, middle row*) occurred often much later than the peak velocity of the cursor translation (*vertical lines, bottom row*), but it then occurred progressively earlier with practice (Blocks 8-16, *yellow lines*).

Mean success rate across participants in target reaching and holding increased during the 12 NSC blocks. Reaching

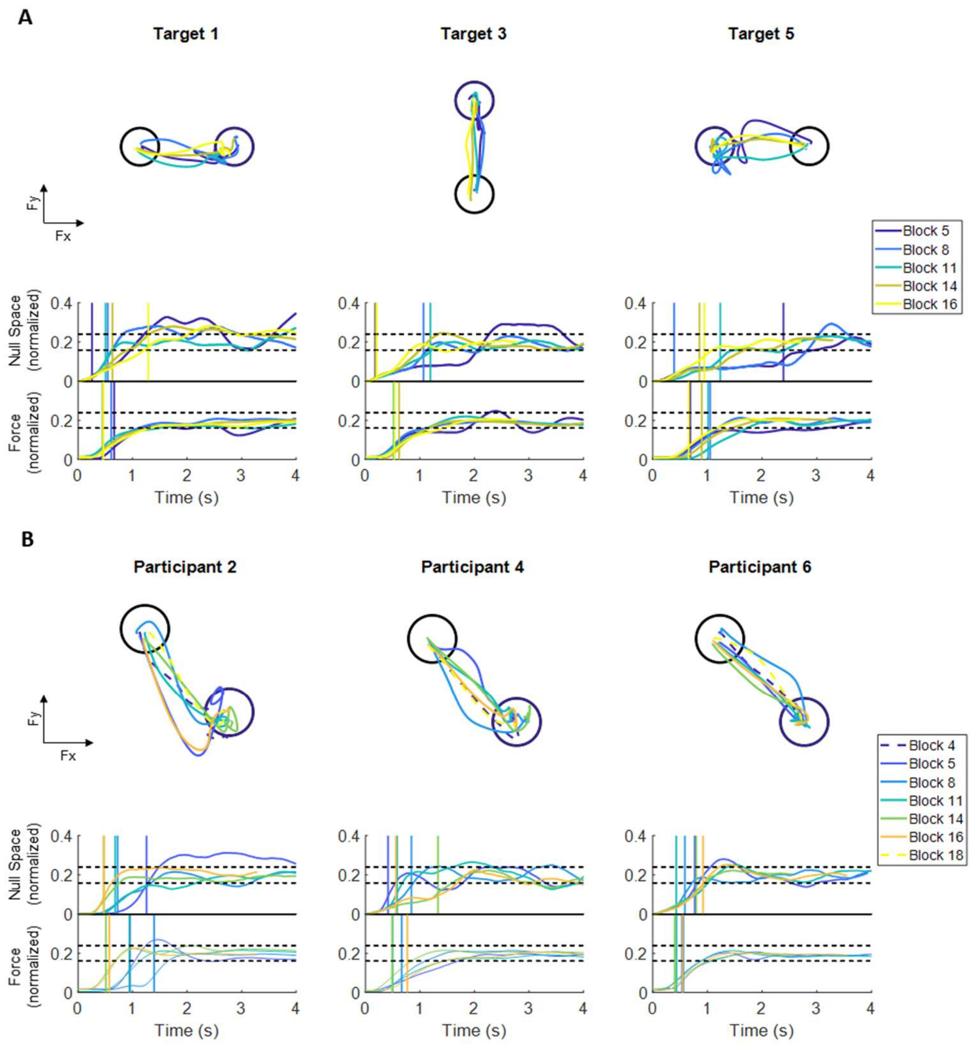

Figure 3. Examples of task performance during NSC blocks. (A) Example of cursor trajectories to different targets (1, 3 and 5) for participant 6: for each target (*column*) the plot on *top* shows the trajectory in F_x-F_y plane (being the target distance expressed in % of the MVF), the *middle* plot shows the evolution in time of the normalized null space control variable, and the plot on *bottom* the normalized force. To illustrate the temporal evolution of trajectories, the color changes with block number: trajectories became straighter over blocks. Vertical lines show the time of first velocity peak. (B) Example of trajectories in the x-y plane (*top row*) and time evolution of null space control variable (*middle row*) and force (*bottom row*) to one target (8), for participants 2, 4, and 6 (*columns*). Trajectories in the *x-y* plane during EFC are also shown for comparison (*dashed lines, top row*). The dashed black lines indicate target tolerance.

success rate progressed from 72 ± 26 % in the first block to 93 ± 11 % in the last block. Holding success rate was initially low, 12 ± 12 % in the first block, and achieved a maximum value of 43 ± 31% (Fig. 4A and B). The mean movement time across participants decreased over blocks, with a starting value of 2.79 ± 0.54 s and an ending value of 2.02 ± 0.54 s. The mean holding time across participants increased, achieving the highest mean value of 0.70 ± 0.29 s, while the mean angular error decreased below the required target threshold of 7.2° (6.69 ± 2.18° for the last block, minimum mean value achieved) (Fig. 4C and D).

A generalized linear mixed model analysis, with cycle (i.e., a subdivision of a block, with three cycles per block) and target as fixed effects and participant as random effect, showed a significant dependence of both reaching and holding success rate on cycle ($p < 0.001$ for both variables, with a slope of 0.047 and 0.041, respectively), indicating a significant increase in average performance with practice. The effect of target was also significant for both reaching and holding (p = 0.001 and 0.041, respectively), which means performances were not equal across targets. In fact, targets 4, 5 and 8 showed lower mean reaching success rate with respect to target 1,

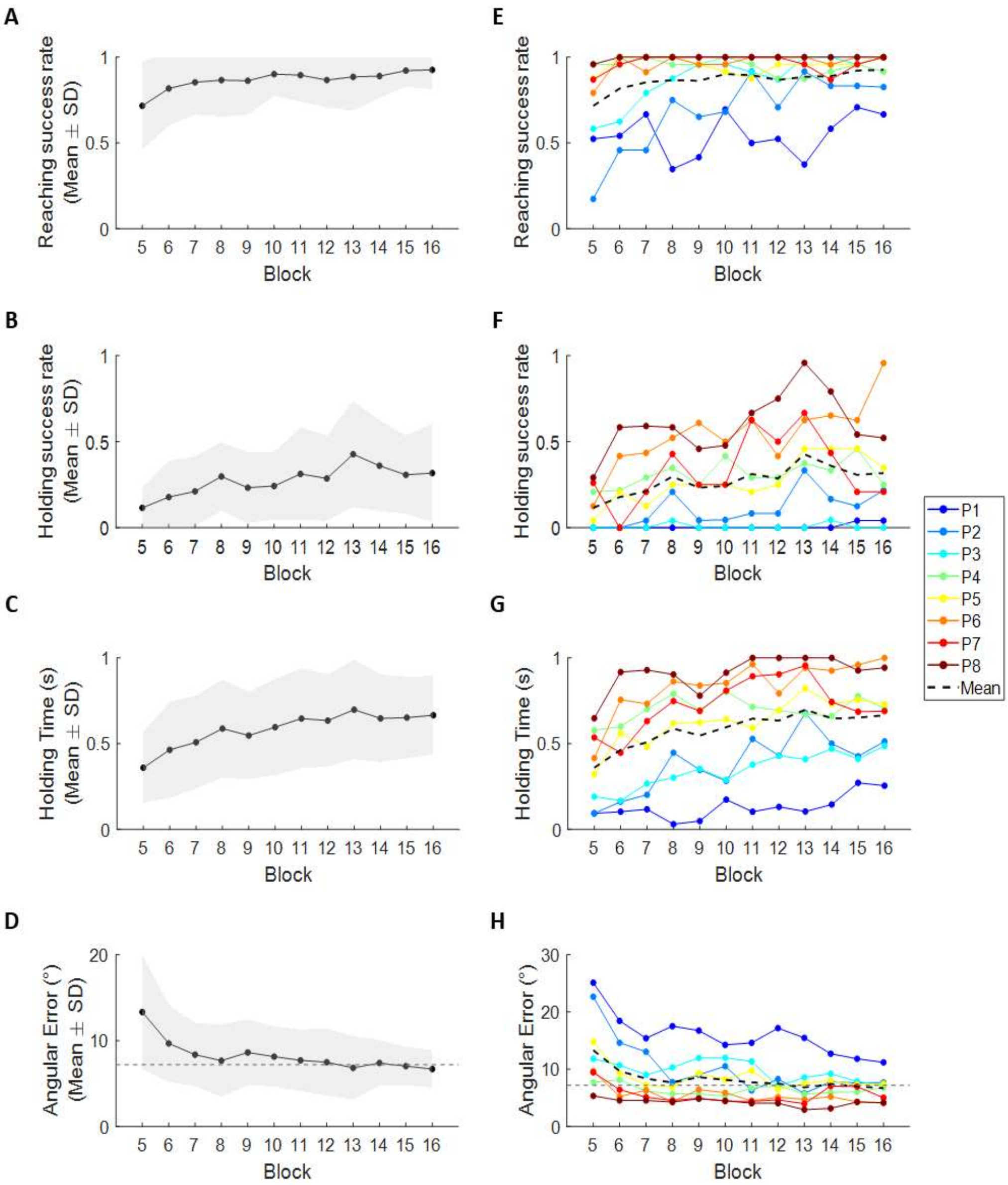

Figure 4. Simultaneous force and null space control performance. The mean values across participants (left column panels) show that reaching success rate (A), holding success rate (B) and holding time (C) increased with practice, while angular error (D) decreased. Right column panels show the curves for each participant separately and make visible the variability in performance among them. Shaded areas represent mean ± SD, and the gray dashed line in panels (D) and (H) represents target tolerance for angular error.

taken as reference ($p = 0.006$, 0.002 and 0.004 respectively), while target 6 presented higher holding success rate ($p = 0.022$).

Remarkably, there was substantial inter-individual variability in performance, especially for target holding, as indicated by the large standard deviation (Fig. 4A, B, C and D). For this reason, we also analyzed the data of individual participants separately, fitting them with a subject-specific generalized linear model with cycle and target as fixed effects. Individual performance curves are plotted in Fig. 4E and F. For reaching success rate, we found a significant effect of cycle only in participants 2, 3 and 6 (Table 2). This is because all the other participants, except participant 1, had high reaching success rate from the beginning of the experiment. Participant 1 was instead rather erratic, with a large variability in success rate from block to block, and always below 80%. For holding success rate, we found a significant effect of cycle for participants 2, 5, 6, 7 and 8 (Table 2). A significant target effect on reaching performance was found for participants 1, 2, 3 and 4 and on holding performance for participants 4, 5, 6, 7 and 8 (Table 3). These results indicate that, with practice, some participants improved their control skills in reaching or in holding while others did not, and that such skills were not equal across the different directions.

Linear mixed models, with cycle and target as fixed effects and subjects as random effect, showed a significant dependence of holding time and angular error on cycle ($p < 0.001$ for both variables, slope 0.009 and -0.12, respectively). Target effect was not significant for holding time ($p = 0.09$), while it was significant for angular error ($p < 0.001$).

Holding time and angular error individual curves are plotted in Fig. 4G and H. Linear models fitted separately to each individual participant showed a significant cycle effect on holding time for all participants except participant 4, while for the angular error a significant cycle effect was found for all participants except participant 4 and 7 (Table 2). Both these participants had values close to their best values since the beginning of the experiment. Target effect on holding time was significant for all participants (while it was not the case when considering them together) and on angular error for all participants except participants 6 and 7 (Table 3). In sum, this analysis highlighted that, even when success rate does not increase significantly, improvements can be observed in continuous parameters such as holding time and angular error.

Subject	Reaching success rate	Holding success rate	Holding time	Angular error
1	0.26	0.17	< 0.001*	< 0.001*
2	< 0.001*	0.002*	< 0.001*	< 0.001*
3	< 0.001*	0.94	< 0.001*	< 0.001*
4	0.14	0.17	0.20	0.10
5	0.65	< 0.001*	< 0.001*	< 0.001*
6	0.005*	< 0.001*	< 0.001*	< 0.001*
7	0.61	0.02*	< 0.001*	0.09
8	0.33	0.003*	< 0.001*	< 0.001*

Table 2: p-values for the effect of cycle on success rate (reaching and holding), holding time and angular error. The asterisk indicates $p < 0.05$.

Subject	Reaching success rate	Holding success rate	Holding time	Angular error
1	< 0.001*	1	0.048*	< 0.001*
2	< 0.001*	0.574	< 0.001*	< 0.001*
3	0.013*	1	0.015*	0.029*
4	0.029*	0.007*	< 0.001*	< 0.001*
5	0.287	< 0.001*	< 0.001*	< 0.001*
6	0.999	< 0.001*	0.001*	0.072
7	0.726	0.005*	0.004*	0.379
8	1	< 0.001*	< 0.001*	< 0.001*

Table 3: p-values for the effect of target on successful trials fraction (reaching and holding), holding time and angular error. The asterisk indicates $p < 0.05$.

We then investigated the force control and the null space control performances separately, i.e., the success rate for reaching and holding considering only either the position or the rotation of the cursor (Fig. 5). The separate performances were better than the combined performance, which was provided as feedback to the participants during the experiment (as the change of color of the target when both position and orientation of the cursor were within the target tolerance). All participants achieved a 100% reaching success rate in at least one block for both force control and null space control separately (maximum mean ± SD across participants: 99.5 ± 1.4 % and 98.9 ± 1.8 %, respectively). Holding success rate raised to 89 ± 12 % for force control, with 4 participants achieving 100%, and 60 ± 32 % for null space control. It was therefore the lack of coordination in displacing and rotating the cursor that significantly affected the global performance.

A generalized linear mixed model analysis highlighted a significant dependence on cycle for both reaching and holding of both force and null space control performance ($p < 0.001$ for all cases, slope of 0.09, 0.05, 0.05 and 0.04 for force reaching, force holding, null space reaching and null space holding respectively). Target effect was significant only for null space reaching ($p < 0.001$), while it was not for force reaching ($p = 0.13$), force holding ($p = 0.15$) and null space holding ($p = 0.58$).

The analysis of the performances of each participant separately revealed different individual strategies, which were not evident when considering success rate for combined force and null space control. For example, participant 1 showed a significant cycle effect in all success rates except null space reaching, showing an improvement not visible with simultaneous control success rate. This participant, together with participant 2, was the only one with a significant improvement in force reaching, while in force holding participants 3, 6 and 7 also showed a significant improvement together with 1 and 2. In null space reaching only participants 2 and 3 had a significant cycle effect; nonetheless, all participants except participant 4 had significant cycle effect in null space holding. It is worth noting that participant 4 increased their performance in null space holding, but after nine blocks, performance started to decrease probably due to fatigue and/or distraction.

In the final EFC block, after the NFC blocks, mean success rates across participants for reaching and holding were respectively 95 ± 12 and 77 ± 24 %. No significant differences

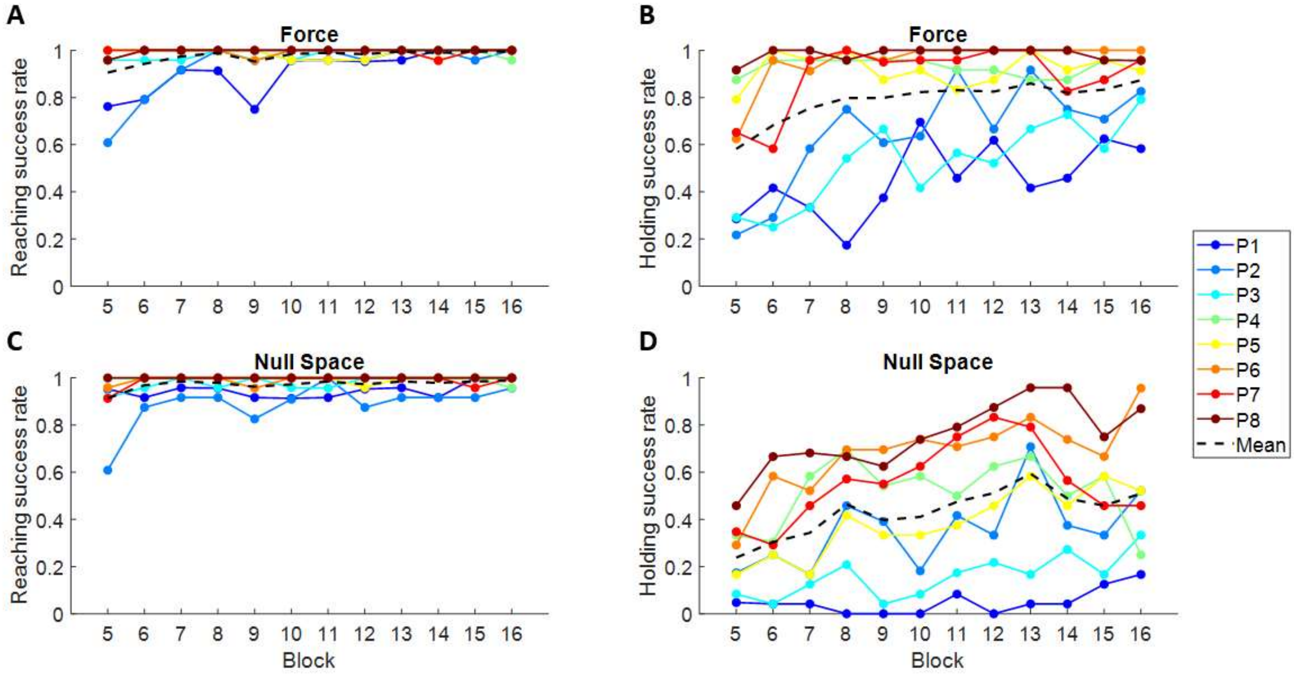

Figure 5. Separate force control and null space control performance. Reaching and holding success rates for force control (*first row*) and null space control (*second row*) are shown separately. The black dashed lines represent mean across participants.

were found between initial and final EFC blocks, for both reaching and holding (p = 0.19 and 0.48, respectively, Kruskal-Wallis one-way ANOVA). This indicates that practicing simultaneous force and null space control did not affect force control alone. The mean horizontal force reconstruction R^2 across participants during the final EFC block was 0.67 ± 0.23, and no significant differences were found with respect to the initial EFC block (p = 0.48, Kruskal-Wallis one-way ANOVA). This suggests that null space control did not affect standard force control patterns even after prolonged practice.

3.3 Peak velocity times and movement strategies

We analyzed peak velocities to better characterize the different strategies of individual participants. Each participant showed a specific timing of the peak velocity for cursor displacement and for cursor rotation. Some participants first rotated the cursor and then displaced it, others first displaced the cursor and then rotated it, and others performed both movements simultaneously. Furthermore, peak velocity times were not constant over blocks, and they decreased or increased depending on the participant and on the specific target. As can be seen in Fig. 6, the high SD values of the peak velocity times in individual blocks indicate a large variability across targets.

Kruskal-Wallis one-way ANOVA, with peak type as factor, was performed to compare translation and rotation peak velocity times of each participant. This revealed a significant difference between the translation and rotation peak velocity times for all participants (p = 0.002 for participant 4, p < 0.001 for participants 1, 3, 5, 7, and 8) except 2 and 6 (p = 0.82 and 0.42 respectively), although participant 6 had a high variability in rotation peak velocity times across targets. It is also worth noting that, among the participants with significant differences between the two times, only participant 4 had significantly earlier rotation velocity peak than displacement velocity peak.

Translation and rotation peak velocity times showed a strong positive correlation across blocks for participants 2 and 5 (Pearson correlation coefficient r = 0.87 and 0.83, respectively) considering all targets directions together, with both mean times decreasing over time (blocks). Moderate positive correlation was found for participants 1 and 6 (r = 0.68 and 0.52, respectively), with both mean times also decreasing over time. Moderate negative correlation was instead found for participant 3 (r = -0.42), with both mean times decreasing up to block 10, after which the rotation peak time increased. Weak negative correlation was found for participant 4 (r = -0.23), while no significant correlation was found for participant 8 (r = 0.09), with a constant displacement peak velocity time and a decreasing rotation peak velocity time.

3.4 Individual null space control ability

Because of the high variability among the participants in the performance metrics that we analyzed, such as success rate and holding time, which depend on task conditions such as target and time tolerances, we wondered if it was possible to generalize the assessment of individual ability in the

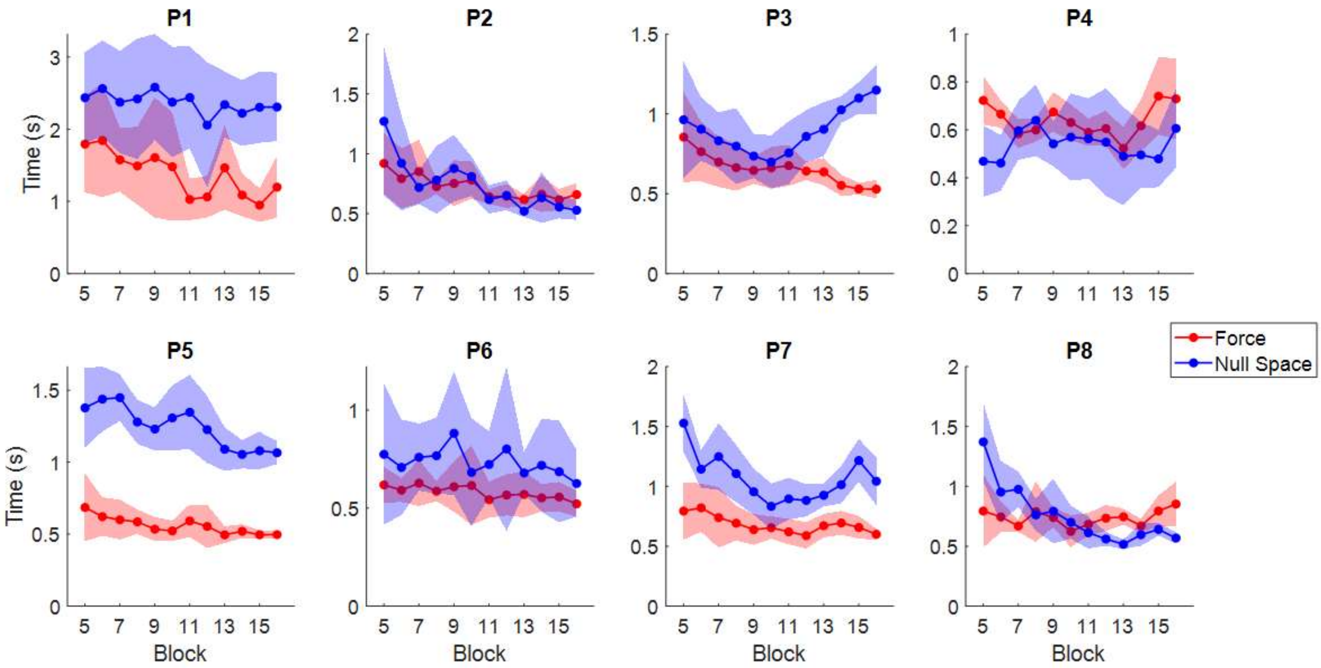

Figure 6. Individual movement strategies. Mean peak velocity times across targets, over null space control blocks, for both force and null space control variables. Shaded area represents standard deviation across targets.

simultaneous control of natural and extra DoFs. To this aim, we used an information theory approach inspired by Fitts' law, with an ID comprising a spatial term for the reaching phase and a temporal term for the holding phase. We also estimated the performance that would have been achieved with different target sizes and holding time tolerances through a simulation.

For the reaching phase only, due to the variability in movement time for the different directions, the linear fit of the movement time itself as a function of the Shannon-MacKenzie ID resulted in a R^2 of 0.26 ± 0.17 (mean ± SD across participants). The linear fit was significant for seven participants ($p < 0.001$ for participants 2 to 8, while $p = 0.41$ for participant 1), which supports the validity of the Fitts' model for reaching. The plot of the corrected spatial ID as a function of the target size (Fig. 7A) shows that the smallest target is not always the one that allows maximizing the transmitted information. While simulated performances appear to be similar for what concerns the largest possible target, decreasing target size does not always lead to an increase in the transmitted information, because the increase in the total available information associated with smaller targets is overcome by a decrease in success rate. This means that a specific target size can maximize information transmitted through reaching, and it is strictly dependent on participants' ability.

On average, the throughput, calculated as the ID divided by the movement time for reaching, increased during NSC blocks (Fig. 7B). This is expected, as the movement time for reaching also decreased among blocks. This result indicates that with practice participants moved faster while keeping good accuracy.

When considering both the reaching and the holding phase, the linear fit of the simulated movement time as a function of combined ID resulted in a mean R^2 of 0.56 ± 0.18, and all fits were significant ($p < 0.001$ for all participants). This means that a linear relation still holds when the ID also includes a temporal term.

Introducing the additional temporal ID generally affects the target size at which a participant can transmit the maximum information, as can be seen in the example of participant 6 illustrated in Fig. 7C. While for the reaching ID (which corresponds to the curve at fixed $\Delta t = \pm 0.999$ s) the best target size was 3.5 % of MVF/MVCC, for holding the best target size was 4 % (the red dot in Fig. 7C), with a Δt of ± 0.1 s (the minimum Δt). Moreover, not all participants had their maximum information transmitted for the same time tolerance, indicating that also this quantity depends on participants' ability in holding the cursor in a fixed position.

Finally, the maximum information transmitted when reaching and holding (i.e., the maximum value of information among all the simulated conditions, Fig. 7D) also increased with practice. This means that participants improved with practice their ability to control concurrently natural and extra DoFs, both spatially and temporally.

4. Discussion

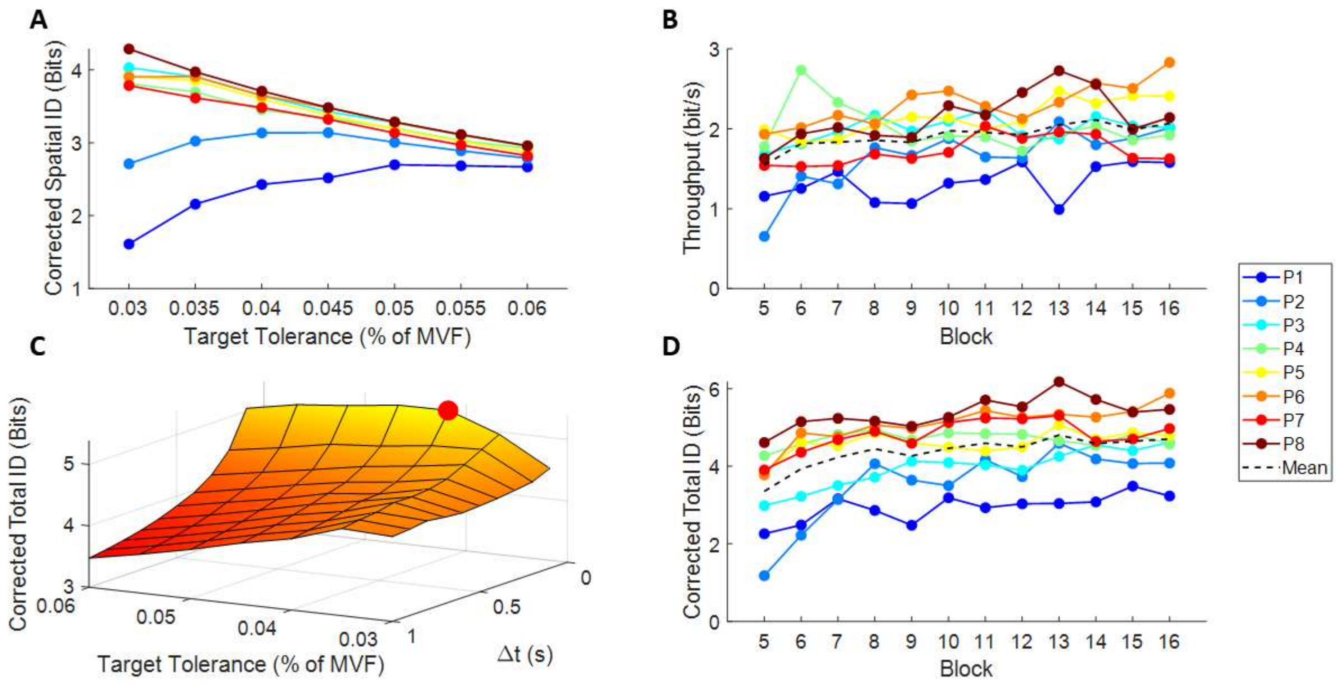

Figure 7. Assessment of individual control ability. (A) The corrected spatial ID (mean among the last three NSC blocks, estimated through a simulation) is shown as a function of target tolerance, showing the optimal target size for reaching of each participant. (B) Throughput as a function of block number. The dashed black line corresponds to the mean value among participants. (C) Example of corrected total ID (mean among the last three NSC blocks) as a function of target and time tolerances for participant 6. The red dot indicates the maximum value of transmitted information achieved by the participant among all the simulated conditions; the temporal evolution of its value is reported in orange curve of panel (D). It is worth noting that other maxima could be present outside the space covered by the simulation, and that the curve for $\Delta t = 0.999\ s$ (reaching condition) is equivalent to the one present in the panel (A). (D) Temporal evolution of the maximum information transmitted (among all the simulated conditions, i.e., the maximum of the surfaces such as that shown in panel (C)) for each block and participant. The dashed black line corresponds to the mean value among participants.

The control of an extra limb or end-effector while simultaneously performing movements with the natural limbs requires using signals that do not interfere with limb motion [26,64]. As a first step towards the ambitious goal of augmenting human motor capabilities, we tested whether simultaneous control of natural and extra DoFs through isometric force and intrinsic muscular null space signals is feasible. We developed a control interface in a virtual environment using isometric force generated at the hand to control the translation of an ellipsoidal cursor and, concurrently, muscle-to-force null space activations, i.e., patterns of muscular activations that do not generate force, to control the rotation of the cursor around one axis. We assessed how well 8 participants controlled the end-effector with such interface in a reaching task that required translating and rotating the cursor to match the position and orientation of ellipsoidal targets, thus testing spatial control, and maintaining the cursor in the target for a 1 s, thus also testing temporal control. The results indicate that such an application of muscular null space is feasible, as after a moderate amount of practice average reaching performance was close to 100%. Furthermore, all the participants showed improvements in different performance parameters with practice, such as an increase in reaching and holding success rate, a reduction of angular error, and an increase of holding time. However, we found remarkable inter-individual differences in task performance, learning capabilities, and strategies to coordinate natural and extra DoFs. We also found significant increases in the median frequency of the EMG spectrum of some muscles, which can be considered indices of fatigue that may have affected performance.

There are three kinds of null spaces that can be defined for the human motor system: kinematic, muscular, and neural [26]. Moreover, when considering null space signals to be used for controlling extra DoF during the performance of a task, we can define as task-*extrinsic* those null space signals generated by body parts, muscles, or neural circuits not directly involved in the task, and task-*intrinsic* those signals directly involved. Here we considered task-intrinsic muscular null space signals for extra DoFs control. Muscular null space may be a convenient choice for augmentation since it represents a trade-off between the desirable (low noise and non-invasiveness) and potentially limiting (low dimensionality) characteristics of the kinematic null space and the desirable (high dimensionality) and limiting (invasiveness) characteristics of the neural null space. A larger dimensionality of the null space is desirable because it allows for more flexibility in the selection of the dimensions to be used for control. Additionally, using intrinsic muscular task null space may avoid interfering with the performance of additional tasks involving other body parts. For example, using null space signal from arm muscles to control extra DoFs participating to the main task performed by the arms (e.g., an extra robotic limb positioning an object being manipulated by hands) may allow to perform secondary tasks such as standing or walking.

Our approach is novel because it is the first time that an intrinsic muscular null space signal extracted from multiple arm muscles is used to control an extra DoF. Many applications of extrinsic [27,65–67] or intrinsic [68] kinematic null space, as well as extrinsic muscular null space [31,69,70] and neural null space [32,71,72] has been proposed in the past. However, the possibility of using intrinsic muscular null space for augmentation has received less attention. A recent study has shown that the muscle projection in the beta-band of spiking activity of motor neurons identified from high-density EMGs electrode from a single muscle could be suitable to control additional DoFs concurrently with natural limb motion [40], but possible interference with other muscles was not directly monitored. Another recent study [39] has demonstrated the possibility of controlling the vertical displacement of a cursor in a 2D environment through co-contraction of two antagonistic muscles (pectoralis major and posterior deltoid) while controlling the horizontal displacement through the reciprocal activity of the two muscles. With respect to these recent studies, our interface allowed to directly test the feasibility of simultaneous control in a scenario closer to real-life, i.e., in a 3D virtual environment, of 3 natural DoFs (cursor translation) and an extra DoF (cursor rotation), for a total of 4 DoFs controlled simultaneously. Moreover, our task-intrinsic muscular null space signal was extracted from many muscles involved in the reaching/holding task. We could assess the interference between the different DoFs and the relative muscle activations, showing that participants could learn to reduce such interference with practice. In principle, our approach could also be extended to the control of multiple extra DoFs by selecting different components in the intrinsic muscular null space. However, further investigation is needed to assess how performance and learning rate depends on the number of extra DoFs.

Because of the high inter-individual variability among the participants, we developed an assessment framework based on information theory inspired by Fitts' law to assess individual control ability independently from the performance observed with specific task parameters. In fact, performance quantities such as success rates are strictly dependent on the specific task conditions used in the assessment. In contrast, evaluating performances in terms of an ID, such as the one proposed in the Fitts' law, allows to generalize an individual's performance and extrapolate it from the specific context, representing them as transmitted information and giving a measure of the effective spatial accuracy limits of a participant. Tasks with larger and closer targets can be easily accomplished with high success rates but low spatial accuracy, which means low information transmitted, i.e., the possibility of choosing a smaller number of targets in a given task. On the other hand, tasks with smaller and farther targets are more difficult, requiring high spatial accuracy which is equivalent to more spatial information transmitted. Since its original formulation [51], Fitts' law has been widely employed to evaluate human performance during tracking [73], myoelectric control [74], prostheses control [75], and human-computer interaction (HCI) [44,52,76]. Fitts' law captures the speed-accuracy tradeoff typically observed in human aimed movements by relating movement duration to an ID defined according to target distance and size. Thus, since the ability to accurately control an end effector depends on the speed of movement, motor control ability should be assessed according to a speed-accuracy trade-off function rather than by accuracy alone [62]. However, the ID itself, corrected through the success rate of a participant, as a measure of average transmitted information [41], can be taken as a metric for performance evaluation related to spatial accuracy and control ability.

While various formulation of Fitts' law have been developed to adapt to different tasks or to correct the ID to account for target misses [41,60,77], Fitts' law has always been considered in the spatial domain, with time taken into account only in the form of temporal constraints influencing task execution [55,56]. However, it may be sometimes necessary to evaluate the performance also in temporal domain, such as to evaluate whether an individual is able to perform an action at the right time or for the required time lapse. To account for the effects of temporal targeting, i.e., a task in which spatial distance is minimal and for this reason movement time can be considered constant and close to zero, a recent study applied Fitts' law to a temporal pointing task, in which the user must only decide when to perform an action (in this case, pressing a button when the cursor is inside targets) [45]. Assuming a Gaussian response distribution for the endpoints, the error rate could be expressed as a function of an ID equal to the logarithm of a temporal target distance divided by a temporal target width. Similarly, to take into account the holding phase in our task, which can be considered a temporal task, we hypothesize that the total information transmitted performing the task is equal to the sum of two IDs, a spatial ID resembling the classical Fitts' index, and a temporal ID similar to the one proposed in [45]. As the Fitts ID can be derived from an “aiming is choosing” rationale [41], we simply derived the temporal ID from a “waiting is choosing” rationale, which allows a generalization of the temporal ID to any compatible temporal task without relying on any assumption on the response function. We also corrected those ID multiplying them for the respective success rate (reaching or holding) [41]. Such ID therefore allows to consider not only reaching tasks, but also holding tasks, and could be hypothetically extended to more complex tasks composed by multiple reaching and holding phases to evaluate an invidual performance based on the average information transmitted in each phase. Through this framework, we found that, when considering only the reaching phase, the smallest target size is not always the one providing the highest information transmitted because the gain in source information associated with smaller targets may be overcome by the loss in transmission performance corresponding to a decrease in reaching success rate. When considering both reaching and holding phases, we found that spatial and temporal requirements affect each other, generally reducing the participants’ optimal target size with respect to the reaching phase only, with the maximum information transmitted resulting for a specific, individual combination of spatial and temporal parameters. Such an approach could allow to hypothetically optimize an interface (not necessarily based on myoelectric control) depending on the user’s capabilities, possibly also adapting the interface parameters as the user learns to control the device.

However, it must be considered that the simulation using such a model, while based on real trajectories of the cursor, has been performed offline after the experiment and the resulting parameters to be used to personalize the interface have not been tested in a subsequent experiment. Therefore, actual performances in real tasks may anyway differ from the predicted ones. Moreover, the range of spatial and temporal tolerances used in the simulation corresponded to a range of uncorrected spatial IDs (3.2-5 bits, considering direction corrections) that was higher than the range of temporal IDs (0.6-2.6 bits). This was determined by the specific task conditions (i.e., distance of the targets at 20% of MVF and holding time at 1 s) which constrained the set of tolerances that could be simulated, and by the fact that the spatial ID is the sum of a displacement ID (range: 1.2-2.3 bits, considering direction corrections) and an angular ID (range: 1.9-2.7 bits). Then, the total ID metric and, consequently, the selection of optimal spatial and temporal tolerances, poses more emphasis on the individual ability of controlling simultaneously natural DoFs and null space DoFs *spatially*, considering reaching and holding simply as separate phases.

The prolonged exposition to the control of both prostheses and augmenting devices may have effects at the neural level. Amputation causes reorganization in the primary somatosensory cortex [78]. A recent study has showed that, in BCI control of independent DoFs, it is possible to dissociate neural gamma activity correlated to muscle activations [71]. Another study has shown that users of a third thumb controlled through a toe presented, after 5 days, a different representation of their hand in the sensorimotor cortex [28]. Considering the findings of such studies, we expect that even the intrinsic muscular null space control of an external device could bring some modifications in neural motor circuits. The exploitation of musculoskeletal redundancy to control a device is actually a new motor skill that requires learning, as it has been shown by the success rate curves from our study, and it is something different from the natural modulation of limb impedance [38] and even from the tele-impedance, which is based on the use of muscular null space to control the impedance of robots, providing them with a task-related elastic profile in addition to position trajectories [36], while no actual additional DoF is controlled. Thus, we hypothesize that, in this context, null space control improvements with training could be associated to the acquisition of novel muscular null space synergies, possibly encoded in the corticospinal pathways [79] and in the cortico-cerebellar circuits [80]. Investigation of the neuroplasticity associated to learning null space control may be necessary to test such a hypothesis.

Another important finding that has been illustrated in literature is that, as for skill learning [81–83], feedback mechanisms integrated in an interface could help users improving their performance faster and to a higher level. It has been demonstrated that somatosensory feedback facilitates to learn controlling both prostheses [84] and augmenting devices [85]. Our protocol did not include any kind of feedback except visual one, and as a future perspective, it could be interesting to test the effect of somatosensory feedback in interfaces based on intrinsic muscular null space and study its effects on learning and control variability.

In conclusion, we demonstrated the feasibility of a novel approach to control extra DoFs using muscular null space signals from many muscles directly involved in a task being performed concurrently. Participants in our experiment were able to reach targets and their performances improved with practice. Such an approach could be applied to control more sophisticated assistive or augmentative robotic devices (as extra limbs) in everyday life situations, for both able-bodied and disable-bodied people. Such approach is substantially different from the myoelectric control of exoskeletons, as they do not add additional DoFs [7,10,21]. We also developed an assessment framework based on information theory inspired by Fitts’ law, with two indices of difficulty, which could be useful to quantify a participant’s ability in reaching and holding a position independently from specific parameters of the assessment task. Further work is needed to understand the neural origin and mechanisms underlying learning of null space control. These results can be a starting point for the investigation of muscular null space control for augmentation, and our information theory approach can provide a novel tool to assess the ability of individual participants to control a device through noisy signals such as EMG, considering not only spatial precision, but also temporal precision.

Acknowledgements

This work was supported by the Italian University Ministry (PRIN grants 2015HFWRYY_001 and PRIN2017CBF8NJ_005) and by the Italian Space Agency (ASI-MARS-PRE DC-VUM-2017-006).

References

[1] Fougner A, Stavdahl Ø, Kyberd P J, Losier Y G and Parker P A 2012 Control of Upper Limb Prostheses: Terminology and Proportional Myoelectric Control—A Review *IEEE Transactions on Neural Systems and Rehabilitation Engineering* **20** 663–77

[2] Ha K H, Varol H A and Goldfarb M 2011 Volitional control of a prosthetic knee using surface electromyography *IEEE Transactions on Biomedical Engineering* **58** 144–51

[3] Huang S, Wensman J P and Ferris D P 2014 An experimental powered lower limb prosthesis using proportional myoelectric control *Journal of Medical Devices, Transactions of the ASME* **8**

[4] Jiang N, Rehbaum H, Vujaklija I, Graimann B and Farina D 2014 Intuitive, Online, Simultaneous, and Proportional Myoelectric Control Over Two Degrees-of-Freedom in Upper Limb Amputees *IEEE Trans. Neural Syst. Rehabil. Eng.* **22** 501–10

[5] Parker P A and Scott R N 1986 Myoelectric control of prostheses *Crit Rev Biomed Eng* **13** 283–310

[6] Vujaklija I, Farina D and Aszmann O 2016 New developments in prosthetic arm systems *ORR* **Volume 8** 31–9

[7] Dollar A M and Herr H 2008 Lower extremity exoskeletons and active orthoses: Challenges and state-of-the-art *IEEE Transactions on Robotics* **24** 144–58

[8] Ferris D P and Lewis C L 2009 Robotic lower limb exoskeletons using proportional myoelectric control *2009 Annual International Conference of the IEEE Engineering in Medicine and Biology Society* 2009 Annual International Conference of the IEEE Engineering in Medicine and Biology Society pp 2119–24

[9] Lunardini F, Casellato C, d'Avella A, Sanger T D and Pedrocchi A 2016 Robustness and Reliability of Synergy-Based Myocontrol of a Multiple Degree of Freedom Robotic Arm *IEEE Transactions on Neural Systems and Rehabilitation Engineering* **24** 940–50

[10] Singh R M and Chatterji S 2012 Trends and Challenges in EMG Based Control Scheme of Exoskeleton Robots - A Review *International Journal of Scientific and Engineering Research* **3** 1–8

[11] Song R, Tong K, Hu X and Zhou W 2013 Myoelectrically controlled wrist robot for stroke rehabilitation *Journal of NeuroEngineering and Rehabilitation* **10** 52

[12] Berger D J, Gentner R, Edmunds T, Pai D K and d'Avella A 2013 Differences in Adaptation Rates after Virtual Surgeries Provide Direct Evidence for Modularity *J. Neurosci.* **33** 12384–94

[13] Rugy A de, Loeb G E and Carroll T J 2012 Muscle Coordination Is Habitual Rather than Optimal *J. Neurosci.* **32** 7384–91

[14] Barnard A and Jackson A 2012 Flexible Cortical Control of Task-Specific Muscle Synergies *J. Neurosci.* **32** 12349–60

[15] Radhakrishnan S M, Baker S N and Jackson A 2008 Learning a Novel Myoelectric-Controlled Interface Task *Journal of Neurophysiology* **100** 2397–408

[16] Sang-Hui Park and Seok-Pil Lee 1998 EMG pattern recognition based on artificial intelligence techniques *IEEE Transactions on Rehabilitation Engineering* **6** 400–5

[17] Young A J, Smith L H, Rouse E J and Hargrove L J 2013 Classification of Simultaneous Movements Using Surface EMG Pattern Recognition *IEEE Transactions on Biomedical Engineering* **60** 1250–8

[18] Amsuess S, Goebel P, Graimann B and Farina D 2015 A Multi-Class Proportional Myocontrol Algorithm for Upper Limb Prosthesis Control: Validation in Real-Life Scenarios on Amputees *IEEE Trans. Neural Syst. Rehabil. Eng.* **23** 827–36

[19] Jiang N, Englehart K B and Parker P A 2009 Extracting Simultaneous and Proportional Neural Control Information for Multiple-DOF Prostheses From the Surface Electromyographic Signal *IEEE Trans. Biomed. Eng.* **56** 1070–80

[20] Vukobratovic M, Borovac B, Surla D and Stokic D 2012 *Biped Locomotion: Dynamics, Stability, Control and Application* (Springer Science & Business Media)

[21] Fleischer C and Hommel G 2008 A Human–Exoskeleton Interface Utilizing Electromyography *IEEE Transactions on Robotics* **24** 872–82

[22] Johnson D C, Repperger D W and Thompson G 1996 Development of a mobility assist for the paralyzed, amputee, and spastic patient *Proceedings of the 1996 Fifteenth Southern Biomedical Engineering Conference* Proceedings of the 1996 Fifteenth Southern Biomedical Engineering Conference pp 67–70

[23] Ambrosini E, Ferrante S, Schauer T, Klauer C, Gaffuri M, Ferrigno G and Pedrocchi A 2014 A myocontrolled neuroprosthesis integrated with a passive exoskeleton to support upper limb activities *Journal of Electromyography and Kinesiology* **24** 307–17

[24] Stein J, Narendran K, McBean J, Krebs K and Hughes R 2007 Electromyography-Controlled Exoskeletal Upper-Limb–Powered Orthosis for Exercise Training After Stroke *American Journal of Physical Medicine & Rehabilitation* **86** 255–61

[25] Colombo G, Joerg M, Schreier R and Dietz V 2000 Treadmill training of paraplegic patients using a robotic orthosis *Journal of rehabilitation research and development* **37** 693–700

[26] Dominijanni G, Shokur S, Salvietti G, Buehler S, Palmerini E, Rossi S, De Vignemont F, d'Avella A, Makin T R, Prattichizzo D and Micera S 2021 The neural resource allocation problem when enhancing human bodies with extra robotic limbs *Nat Mach Intell* **3** 850–60

[27] Abdi E, Burdet E, Bouri M, Himidan S and Bleuler H 2016 In a demanding task, three-handed manipulation is preferred to two-handed manipulation *Sci Rep* **6** 21758

[28] Kieliba P, Clode D, Maimon-Mor R O and Makin T R 2021 Robotic hand augmentation drives changes in neural body representation *Science Robotics* **6**

[29] Prattichizzo D, Malvezzi M, Hussain I and Salvietti G 2014 The Sixth-Finger: A modular extra-finger to enhance human hand capabilities *The 23rd IEEE International Symposium on Robot and Human Interactive Communication* The 23rd IEEE International Symposium on Robot and Human Interactive Communication pp 993–8

[30] Salvietti G, Hussain I, Cioncoloni D, Taddei S, Rossi S and Prattichizzo D 2017 Compensating Hand Function in Chronic Stroke Patients Through the Robotic Sixth Finger *IEEE Transactions on Neural Systems and Rehabilitation Engineering* **25** 142–50

[31] Parietti F and Asada H H 2017 Independent, voluntary control of extra robotic limbs *2017 IEEE International Conference on Robotics and Automation (ICRA)* 2017 IEEE International Conference on Robotics and Automation (ICRA) (Singapore, Singapore: IEEE) pp 5954–61

[32] Penaloza C I and Nishio S 2018 BMI control of a third arm for multitasking *Science Robotics* **3** 1–6

[33] Burdet E, Osu R, Franklin D W, Milner T E and Kawato M 2001 The central nervous system stabilizes unstable dynamics by learning optimal impedance *Nature* **414** 446–9

[34] Milner T E 2002 Adaptation to destabilizing dynamics by means of muscle cocontraction *Exp Brain Res* **143** 406–16

[35] Selen L P J, Franklin D W and Wolpert D M 2009 Impedance Control Reduces Instability That Arises from Motor Noise *J. Neurosci.* **29** 12606–16

[36] Ajoudani A, Tsagarakis N G and Bicchi A 2012 Tele-impedance: Towards transferring human impedance regulation skills to robots *2012 IEEE International Conference on Robotics and Automation* 2012 IEEE International Conference on Robotics and Automation pp 382–8

[37] Laghi M, Ajoudani A, Catalano M G and Bicchi A 2020 Unifying bilateral teleoperation and tele-impedance for enhanced user experience *The International Journal of Robotics Research* **39** 514–39

[38] Borzelli D, Cesqui B, Berger D J, Burdet E and d'Avella A 2018 Muscle patterns underlying voluntary modulation of co-contraction *PLOS ONE* **13** e0205911

[39] Takagi A, Kambara H and Koike Y 2020 Independent control of cocontraction and reciprocal activity during goal-directed reaching in muscle space *Sci Rep* **10** 22333

[40] Bräcklein M, Ibáñez J, Barsakcioglu D Y and Farina D 2021 Towards human motor augmentation by voluntary decoupling beta activity in the neural drive to muscle and force production *J. Neural Eng.* **18** 016001

[41] Gori J, Rioul O and Guiard Y 2018 Speed-Accuracy Tradeoff: A Formal Information-Theoretic Transmission Scheme (FITTS) *ACM Trans. Comput.-Hum. Interact.* **25** 27:1-27:33

[42] Kamavuako E N, Scheme E J and Englehart K B 2014 On the usability of intramuscular EMG for prosthetic control: A Fitts' Law approach *Journal of Electromyography and Kinesiology* **24** 770–7

[43] Soukoreff R W and MacKenzie I S 2009 An informatic rationale for the speed-accuracy trade-off *2009 IEEE International Conference on Systems, Man and Cybernetics* 2009 IEEE International Conference on Systems, Man and Cybernetics - SMC (San Antonio, TX, USA: IEEE) pp 2890–6

[44] Soukoreff R W and MacKenzie I S 2004 Towards a standard for pointing device evaluation, perspectives on 27 years of Fitts' law research in HCI *International Journal of Human-Computer Studies* **61** 751–89

[45] Lee B and Oulasvirta A 2016 Modelling Error Rates in Temporal Pointing *Proceedings of the 2016 CHI Conference on Human Factors in Computing Systems* CHI '16 (San Jose, California, USA: Association for Computing Machinery) pp 1857–68

[46] Berger D J and d'Avella A 2014 Effective force control by muscle synergies *Front. Comput. Neurosci.* **8**

[47] Hermens H J, Freriks B, Merletti R, Stegeman D, Blok J, Rau G, Disselhorst-Klug C and Hägg G European Recommendations for Surface ElectroMyoGraphy 4

[48] Borzelli D, Gurgone S, De Pasquale P, Berger D J and d'Avella A 2019 Consistency of Myoelectric Control Across Multiple Sessions *Converging Clinical and Engineering Research on Neurorehabilitation III* Biosystems & Biorobotics ed L Masia, S Micera, M Akay and J L Pons (Cham: Springer International Publishing) pp 1166–70

[49] Borzelli D, Burdet E, Pastorelli S, d'Avella A and Gastaldi L 2020 Identification of the best strategy to command variable stiffness using electromyographic signals *J. Neural Eng.* **17** 016058

[50] Merletti R and Parker P J 2004 *Electromyography: Physiology, Engineering, and Non-Invasive Applications* (John Wiley & Sons)

[51] Fitts P M 1954 The information capacity of the human motor system in controlling the amplitude of movement *Journal of Experimental Psychology* **47** 381–91

[52] MacKenzie I S 1992 Fitts' Law as a Research and Design Tool in Human-Computer Interaction *Human–Computer Interaction* **7** 91–139

[53] Meyer D E, Keith-Smith J E, Kornblum S, Abrams R A and Wright C E 1990 Speed-accuracy tradeoffs in aimed movements: Toward a theory of rapid voluntary action *Attention and performance 13: Motor representation and control* (Hillsdale, NJ, US: Lawrence Erlbaum Associates, Inc) pp 173–226

[54] Newell A 1994 *Unified Theories of Cognition* (Harvard University Press)

[55] Carlton L G 1994 The Effects of Temporal-Precision and Time-Minimization Constraints on the Spatial and Temporal Accuracy of Aimed Hand Movements *Journal of Motor Behavior* **26** 43–50

[56] Zelaznik H N, Mone S, McCabe G P and Thaman C 1988 Role of temporal and spatial precision in determining the nature of the speed-accuracy trade-off in aimed-hand movements *Journal of Experimental Psychology: Human Perception and Performance* **14** 221–30

[58] Cha Y and Myung R 2013 Extended Fitts' law for 3D pointing tasks using 3D target arrangements *International Journal of Industrial Ergonomics* **43** 350–5

[59] Murata A and Iwase H 2001 Extending Fitts' law to a three dimensional pointing task *Human Movement Science* **20** 791–805

[60] Welford A T 1968 *Fundamentals of skill* (New York, NY, US: Methuen)

[61] Welford A T 1960 The measurement of sensory-motor performance: Survey and reappraisal of twelve years' progress *Ergonomics* **3** 189–230

[62] Reis J, Schambra H M, Cohen L G, Buch E R, Fritsch B, Zarahn E, Celnik P A and Krakauer J W 2009 Noninvasive cortical stimulation enhances motor skill acquisition over multiple days through an effect on consolidation *PNAS* **106** 1590–5

[63] Shmuelof L, Krakauer J W and Mazzoni P 2012 How is a motor skill learned? Change and invariance at the levels of task success and trajectory control *Journal of Neurophysiology* **108** 578–94

[64] Makin T R, de Vignemont F and Faisal A A 2017 Neurocognitive barriers to the embodiment of technology *Nature Biomedical Engineering* **1** 1–3

[65] Noccaro A, Eden J, Di Pino G, Formica D and Burdet E 2021 Human performance in three-hands tasks *Sci Rep* **11** 9511

[66] Saraiji M Y, Sasaki T, Kunze K, Minamizawa K and Inami M 2018 MetaArms: Body Remapping Using Feet-Controlled Artificial Arms *The 31st Annual ACM Symposium on User Interface Software and Technology - UIST '18* The 31st Annual ACM Symposium (Berlin, Germany: ACM Press) pp 65–74

[67] Kieliba P, Clode D, Maimon-Mor R O and Makin T R 2020 Neurocognitive consequences of hand augmentation *bioRxiv* 2020.06.16.151944

[68] Guggenheim J, Hoffman R, Song H and Asada H H 2020 Leveraging the Human Operator in the Design and Control of Supernumerary Robotic Limbs *IEEE Robotics and Automation Letters* **5** 2177–84

[69] Salvietti G, Hussain I, Cioncoloni D, Taddei S, Rossi S and Prattichizzo D 2017 Compensating Hand Function in Chronic Stroke Patients Through the Robotic Sixth Finger *IEEE Transactions on Neural Systems and Rehabilitation Engineering* **25** 142–50

[70] Guggenheim J W, Parietti F, Flash T and Asada H H 2020 Laying the Groundwork for Intra-Robotic-Natural Limb Coordination: Is Fully Manual Control Viable? *J. Hum.-Robot Interact.* **9** 18:1-18:12

[71] Bashford L, Wu J, Sarma D, Collins K, Rao R P N, Ojemann J G and Mehring C 2018 Concurrent control of a brain–computer interface and natural overt movements *J. Neural Eng.* **15** 066021

[72] Milovanovic I, Robinson R, Fetz E E and Moritz C T 2015 Simultaneous and independent control of a brain-computer interface and contralateral limb movement *Brain-Computer Interfaces* **2** 174–85

[73] Hoffmann E R 1991 Capture of moving targets: a modification of Fitts' Law *Ergonomics* **34** 211–20

[74] Borish C N, Bertucco M and Sanger T D 2020 Effect of target distance on controllability for myocontrol *International Journal of Human-Computer Studies* **140** 102432

[75] Mendez V, Iberite F, Shokur S and Micera S 2021 Current Solutions and Future Trends for Robotic Prosthetic Hands *Annu. Rev. Control Robot. Auton. Syst.* **4** 595–627

[76] Card S K, English W K and Burr B J 1978 Evaluation of Mouse, Rate-Controlled Isometric Joystick, Step Keys, and Text Keys for Text Selection on a CRT *Ergonomics* **21** 601–13

[77] Crossman E 1957 The speed and accuracy of simple hand movements *The nature and acquisition of industrial skills*

[78] Makin T R and Flor H 2020 Brain (re)organisation following amputation: Implications for phantom limb pain *NeuroImage* **218** 116943

[79] Overduin S A, d'Avella A, Carmena J M and Bizzi E 2012 Microstimulation Activates a Handful of Muscle Synergies *Neuron* **76** 1071–7

[80] Berger D J, Masciullo M, Molinari M, Lacquaniti F and d'Avella A 2020 Does the cerebellum shape the spatiotemporal organization of muscle patterns? Insights from subjects with cerebellar ataxias *Journal of Neurophysiology* **123** 1691–710

[81] Morris D, Tan H, Barbagli F, Chang T and Salisbury K 2007 Haptic Feedback Enhances Force Skill Learning *Second Joint EuroHaptics Conference and Symposium on Haptic Interfaces for Virtual Environment and Teleoperator Systems (WHC'07)* Second Joint EuroHaptics Conference and Symposium on Haptic Interfaces for Virtual Environment and Teleoperator Systems (WHC'07) pp 21–6

[82] Wolpert D M, Miall R C and Kawato M 1998 Internal models in the cerebellum *Trends in Cognitive Sciences* **2** 338–47

[83] Wulf G, Shea C H and Matschiner S 1998 Frequent Feedback Enhances Complex Motor Skill Learning *Journal of Motor Behavior* **30** 180–92

[84] Stepp C E, An Q and Matsuoka Y 2012 Repeated training with augmentative vibrotactile feedback increases object manipulation performance *PLoS ONE* **7**

[85] Amoruso E, Dowdall L, Kollamkulam M T, Ukaegbu O, Kieliba P, Ng T, Dempsey-Jones H, Clode D and Makin T R 2021 Somatosensory signals from the controllers of an extra robotic finger support motor learning *bioRxiv* 2021.05.18.444661